Absolute Positioning Using the Earth's Magnetic Anomaly Field†

AARON CANCIANI and JOHN RAQUET
Air Force Institute of Technology, OH, USA

Received April 2015; Revised June 2015

ABSTRACT: *Achieving worldwide dependable alternatives to the Global Positioning System is a challenging engineering problem. Current Global Positioning System alternatives often suffer from limitations such as where and when the systems can operate. Navigation using Earth's magnetic anomaly field, which is globally available at all times, shows promise to overcome many of these limitations. We present a navigation framework that uses Earth's magnetic anomaly field as a navigation signal to aid an inertial navigation system in an aircraft. The filter utilizes ultra-accurate optically pumped cesium magnetometers to make scalar intensity measurements of Earth's magnetic field and compare them with a map using a particle filter approach. The accuracy of these measurements allows observability of not only the inertial navigation system errors but also the temporal effects of Earth's magnetic field, which corrupt the navigation signal. These temporal effects are thoroughly analyzed, and we present a simple model that allows near worldwide use of the navigation filter. We analyze the dependencies on altitude and magnetic storm activity in a realistic simulation using data from test flights and magnetic observatories. Published 2016. This article is a U.S. Government work and is in the public domain in the USA.*

INTRODUCTION

Map-based navigation using magnetic field measurements is not a new concept. Much work has been done in the area of indoor navigation [1, 2]. Magnetic fields can be highly time varying while indoors, making magnetic navigation difficult. Outdoor ground vehicle navigation was explored by Shockley [3]. The effects of man-made noise in this case are still problematic, as demonstrated by large variations observed in repeated ground tracks. Aerial navigation has the benefit of being much further away from manmade sources. These sources still corrupt measurements, but to a much lesser extent. Absolute positioning using Earth's magnetic field is a proven technique with satellites [4]. However, the obtainable accuracies, on the order of tens of kilometers, are not suitable for aerial navigation. This is due to the low spatial-frequency content of Earth's magnetic field at satellite altitudes. The act of increasing altitude essentially acts as a low pass filter on Earth's magnetic field. This loss of frequency information degrades navigation accuracy, which is why at satellite altitudes navigation accuracy using magnetic fields is so low. Aerial navigation experiences the benefits of both being farther removed from manmade sources while simultaneously being in the presence of high spatial-frequency magnetic fields. Furthermore, magnetic anomaly maps, which capture the highest frequency components of Earth's magnetic field, are widely available around the globe. The United States has 100 percent coverage with resolutions ranging from 50 m to 8 km. Several prominent projects have been undertaken to merge the data into continental and world-sized maps. The North American Magnetic Anomaly Database consists of a 1-km resolution map at a 305-m altitude. The World Magnetic Anomaly Model consists of a 3 arc-min resolution map at a 5-km altitude. It is expected that the best navigation accuracy would be obtained over a regional high-resolution map with accuracy degrading using the lower resolution continental and world maps.

Absolute positioning in aerial navigation is relatively unexplored. Wilson and Kline-Schoder [5] used US Geological Survey maps to attempt aerial navigation and obtained accuracies on the order of kilometers. A limitation in Wilson's approach was the use of vector magnetometers. While providing three-axis information, the accuracy of the sensor data is one to two orders of magnitude less than current magnetic intensity sensors. Optically pumped cesium (OPC) magnetometers, for example, have an accuracy of 1nT and are the instruments used for creating magnetic anomaly maps in geological surveys [6]. The results of our research demonstrate that map-based navigation with OPC magnetometers is a superior approach for aerial navigation. Various authors have discussed map-based

†Correction added on 20 July 2016 after online and print publication: The copyright line has been changed from "Copyright Institute of Navigation" to "Published 2016. This article is a U.S. Government work and is in the public domain in the USA".

NAVIGATION: *Journal of The Institute of Navigation*
Vol. 63, No. 2, Summer 2016
Printed in the U.S.A.

positioning using magnetic anomalies from an algorithmic viewpoint, without discussing many practical engineering challenges which would exist in a real system [7–9]. These challenges include the existence of temporal variations in Earth's magnetic field as well as strong altitude dependencies and feasibility in magnetic storm conditions.

One motivator for the exploration of magnetic anomaly navigation is the proven success of terrain contour matching navigation systems such as TERCOM/SITAN [10]. Similar to terrain elevation maps, magnetic anomaly maps contain high spatial-frequency features. Measurements of terrain elevation or magnetic intensity can be made over time and matched to their respective maps. There are several key differences between the phenomenology of terrain contour matching systems and magnetic anomaly systems that drive the development of an effective magnetic anomaly navigation framework. The first is the fact that Earth's magnetic anomaly field is a potential field that varies not only horizontally, but vertically as well. This means the map used for navigation must be three dimensional. This does not add a substantial burden to the navigation system because magnetic potential fields satisfy Laplace's equation [11]. This means a large enough two-dimensional map contains all the information needed to recalculate the map at higher altitudes. This property of potential fields is necessary because existing magnetic anomaly maps are usually created at a set altitude, and it would not be feasible to perform three-dimensional mapping of Earth's magnetic anomaly field. The process of recalculating the map at a higher altitude is known as upward continuation and is discussed further in the Results section of this paper.

A second key difference in the phenomenology of magnetic anomaly navigation is the ability to have a *continuous* map. A terrain elevation map is a grid of values, where each value is an average over a given area. With the data collected from the Shuttle Radar Topography Mission, the resolution of terrain maps are generally 30 m or better. A magnetic anomaly map is simply a grid of measurements as well. However, if the map was adequately sampled when created, an interpolation between points is an accurate reconstruction of the true signal. This is because magnetic anomaly maps are potential fields, and the Nyquist rate to fully sample the field is a simple function of altitude – if grid points are separated by a distance of less than half the altitude, 99.97 percent of total signal energy is captured [12]. This attribute of magnetic anomaly maps is useful for separating out noise from the measurements. If an aircraft flying with a terrain elevation system flew over a large building, this would appear as measurement noise because the height of the building is likely not captured in an elevation map. When flying with a magnetic anomaly map, corrupting effects such as high-frequency ionospheric sources can be separated from the measurements because the filter 'knows' that the fully sampled map cannot contain these frequencies. The separability of corrupting sources from the magnetic anomaly measurements is a key finding in this research.

Another difference in the phenomenology of magnetic anomaly navigation is the availability of the signal. Terrain systems can only operate over the one-third of Earth covered by land. High-frequency spatial features in the magnetic anomaly field exist over both land and water. This is also true for desert-like environments with very little terrain-height variation – magnetic anomaly maps still contain the needed high-spatial frequency content needed to navigate. The high availability of the magnetic anomaly signal applies to time and weather as well – a magnetic measurement is not effected by either of these variables. Alternative systems such as vision-aided navigation systems often rely on daylight and weather conditions to operate. Another benefit of magnetic anomaly navigation is the fact that the instrumentation for making magnetic measurements is mature. OPC magnetometers are extremely accurate absolute instruments. Gravity gradiometry systems are limited by the relatively poor accuracy of existing sensors [13]. Finally, jamming a magnetic anomaly navigation system would be more difficult than jamming radio frequency (RF)-based navigation systems. Magnetic anomaly maps are often accurately modeled as a a grid of magnetic dipoles. When moving away from an RF source, signals decrease in magnitude at a rate of r^2. When moving away from a magnetic dipole, the magnitude of the signal decreases as a rate of r^5 [14].

This paper begins by presenting a background of Earth's magnetic field with a focus on the time varying aspects of the field. We discuss the feasibility of observing the crustal field in the presence of these temporal variations. Through this analysis, we propose a navigation filter that has observability of not only the errors in an inertial navigation system (INS), but also the temporal variations themselves. We then describe the setup of a realistic simulation that uses flight test data as well as actual temporal variations recorded on both magnetically quiet and stormy days. This simulation is used to test the proposed navigation framework with respect to changes in altitude and magnetic storm conditions.

BACKGROUND

Earth's Internal Magnetic Field

Earth's magnetic field is the superposition of a large variety of magnetic sources. The origin and interaction of each of these sources is complex. At

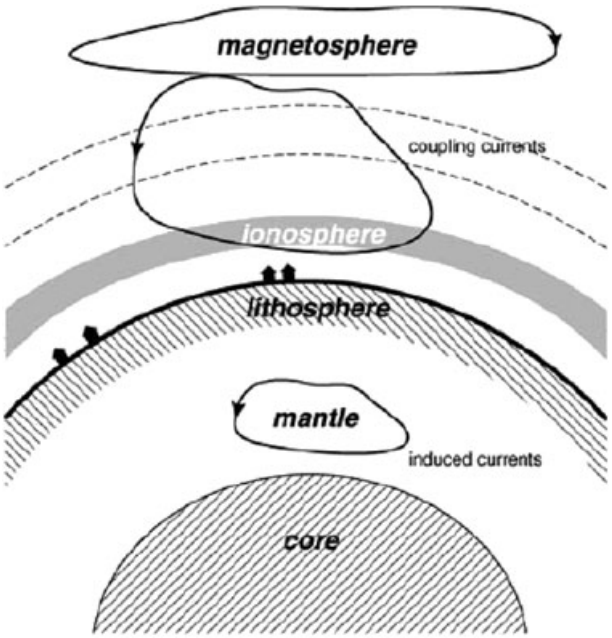

Fig. 1–Magnetic sources of the Earth [15]

a high level, Earth's magnetic field can be thought of as consisting of internal and external sources. The internal sources consist of the core, crustal, and induced fields. The external sources consist of the ionosphere, magnetosphere, and coupling currents. Figure 1 shows these components of Earth's magnetic field. The first component of the internal magnetic field is the core, or main Earth field. The main Earth field is what makes a compass point north. As a first-order approximation, it is a dipole. It accounts for the vast majority of the measured magnetic field near the surface of Earth. It is caused by the motion of conductive fluids deep within Earth. Heat from Earth's inner core causes fluid movement in the liquid outer core, and Earth's rotation causes this fluid to rotate. The rotating conductive materials generate electrical fields, which in turn generate magnetic fields. The field caused by these deep sources accounts for around 95–99 percent of the total measured field at any point in the vicinity of Earth's surface [16]. The magnitude of the main Earth field varies widely and is on the order of tens of micro-teslas. The main Earth field undergoes secular variations. These are variations in the field over time. The changes to the main field are not insignificant – the field is remodeled every five years to account for observed changes [16]. The wavelengths associated with the core field are long. Spherical harmonic models of the core field generally include the first 13 wave numbers of the magnetic field [16]. This indicates that the shortest spatial wavelength that exists as a result of the core field is around 4,000 km. Intuitively, such a low-frequency signal would not allow sub-kilometer level navigation.

External sources will induce currents in the conductive mantle of Earth. These currents in turn will create their own magnetic fields. Although these currents exist deep within Earth, it is important to differentiate them from the main Earth field. Separating these components can often be difficult. These fields are time varying due to the time-varying nature of the external sources that induce them. Models of a region's ground conductivity can help in predicting the effect of induced magnetic fields [17].

The final component of the internal sources is the crustal, or lithosphere field. The crustal sources are caused by the permanent or induced magnetization of rocks in Earth's crust. Because of the lower temperatures of Earth's crust, many magnetic materials are at a temperature below the Curie point [15] – the point at which materials change from having induced magnetization to permanent magnetization. There are two main causes for the mineral's magnetization. The first is remnant magnetization. This is caused by a past induced magnetic field changing to a permanent magnetic field when the mineral cooled below the Curie temperature [15]. The second type of magnetization is induced magnetization. This occurs when the present-day magnetic field induces a magnetic field in the minerals. The magnetic field generated by these sources is small compared to the deep sources. The crustal field accounts for around 1–5 percent of the total measured magnetic field in the vicinity of Earth's surface [17]. This amounts to several hundred nT. An important aspect of the crustal field is that it changes so slowly it may be considered static. It also includes high spatial-frequency information. This makes it an ideal candidate for map-based navigation. An approximation for the shortest expected crustal field wavelengths is simply the measurement altitude. Flying at 1 km altitude, spatial magnetic field wavelengths of 1 km or longer are expected to exist [18]. As altitude increases, individual magnetic features tend to 'blur' together. Increasing altitude thus acts like a low-pass filter on the crustal magnetic field. Intuitively, this indicates altitude will be a major factor in navigation performance.

Earth's External Magnetic Field

The combined effect on the measured magnetic field of all external sources is often referred to as the temporal variations. Temporal variations are caused by many distinct sources with varying characteristics. The amplitude and frequency content of the variations can vary dramatically. As a general rule, higher-frequency variations tend to have lower amplitudes as shown in Figure 2. From a navigation standpoint, this is beneficial, as the larger temporal variations will vary more slowly with time. Slowly changing variations tend to look like

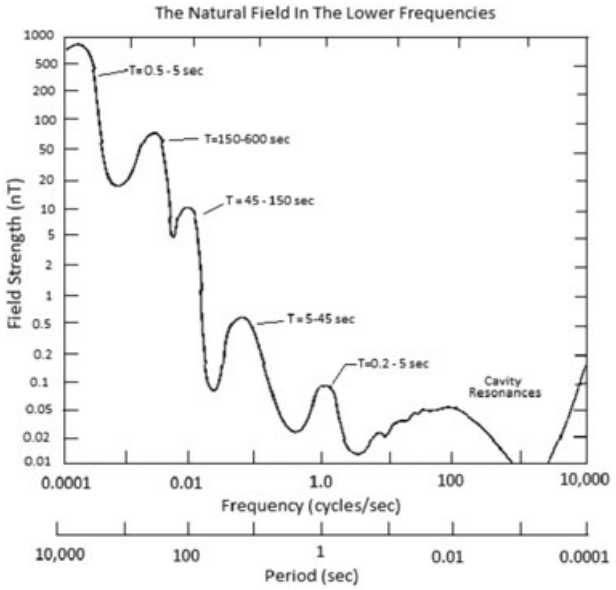

Fig. 2–Frequency content vs. amplitude of Earth's magnetic field [18]

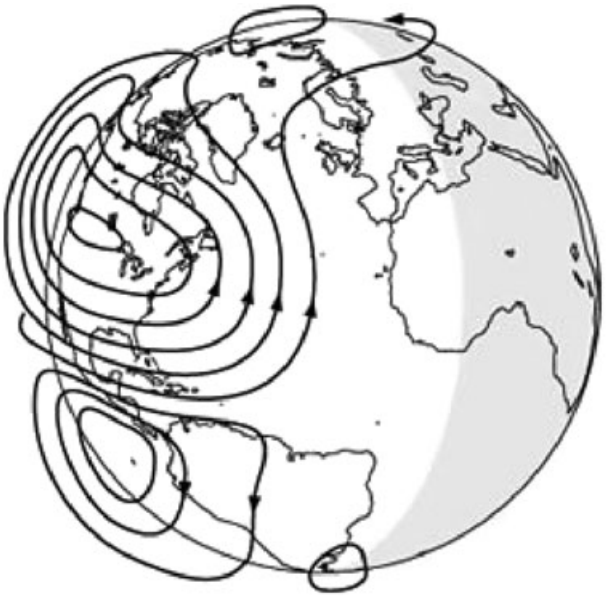

Fig. 3–Solar quiet (Sq) currents on day side of Earth

constant biases over short duration flights. Constant bias type errors are often easier to estimate and correct than time-varying errors. On the opposite end of the spectrum, very high-frequency variations are also not as problematic for a navigation system. High-frequency errors will tend to average out, or appear as white noise. When flying over a spatial map, the spatial-frequency information of the map is transformed to a temporal frequency dependent on flight velocity. Intuitively, temporal variations that occur at similar frequencies to those that exist in the map data will be the most difficult errors to estimate and remove.

The ionosphere is a major contributor to the temporal variations. The ionosphere is ionized by solar radiation, which creates an electrically conducting plasma where electric currents can flow. The flow of these currents is primarily driven by the heating of the atmosphere by the sun. The day–night cycle creates differential solar heating, which causes atmospheric tidal winds. The gravitational attraction of the moon can also create these tidal winds. As the electrically conducting plasma moves relative to the main Earth magnetic field, electric currents are created. These currents in turn create magnetic fields. Figure 3 shows these currents flowing on the day side of Earth. The magnetic field induced as a result of the differential solar heating is called the Sq, or solar quiet variations. Sometimes the currents, which create these variations, are referred to as solar currents. The currents caused by the gravitational attraction of the moon are called lunar currents. The magnetic field caused by the solar and lunar currents is relatively smooth and periodic because these systems exist directly between the sun and Earth, and Earth is rotating. The period of the solar currents is 24 h. The strength of the magnetic field induced by the solar currents depends on latitude, season, and time of day. At the middle latitudes, the solar currents can cause variations of 20 to 40 nT. Near the magnetic equator, these variations can be as high as 100–200 nT as a result of the equatorial electrojet (described below). The lunar currents have a period of 12 h. They cause magnetic field variations of around nT – much smaller than the solar currents [19].

The equatorial electrojet (EEJ) is an eastward current on the day-time side of Earth flowing along the magnetic dip equator. The previously described solar currents cause an east–west directed electrostatic field, which interacts with the magnetic dip equator. The magnetic dip equator is the point at which the main Earth geomagnetic field is horizontal. The resultant current is a narrow band (about 6 deg of latitude) in the equatorial regions. The EEJ can induce magnetic fields 5–10 times stronger than the mid-latitude solar currents. Similar to the solar and lunar currents, the EEJ manifests itself as a 24-h period with respect to stationary measurements taken near the magnetic equator. Like the solar currents, the EEJ is driven by the time of day, season, and solar activity. This indicates that magnetic measurements near the equator will have stronger Sq variations than at mid latitudes. Figure 4 shows the relative strengths of these solar quiet fields. The Sq arrows are pointing to approximately noon local time [19].

The final major ionospheric current systems are the auroral currents. These currents are caused by polar electrojets and other transient currents. They are usually located above 67 deg latitude but may occur lower. The auroral currents have a

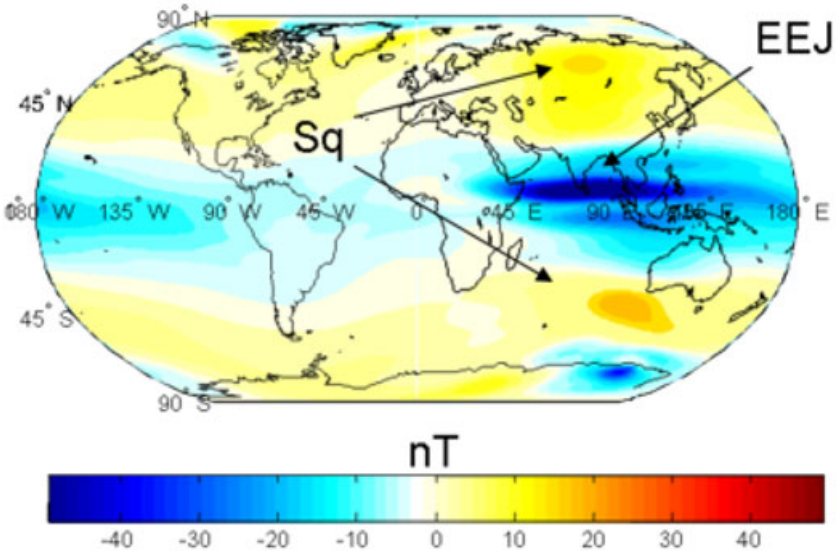

Fig. 4–Solar quiet (Sq) currents on day side of Earth.

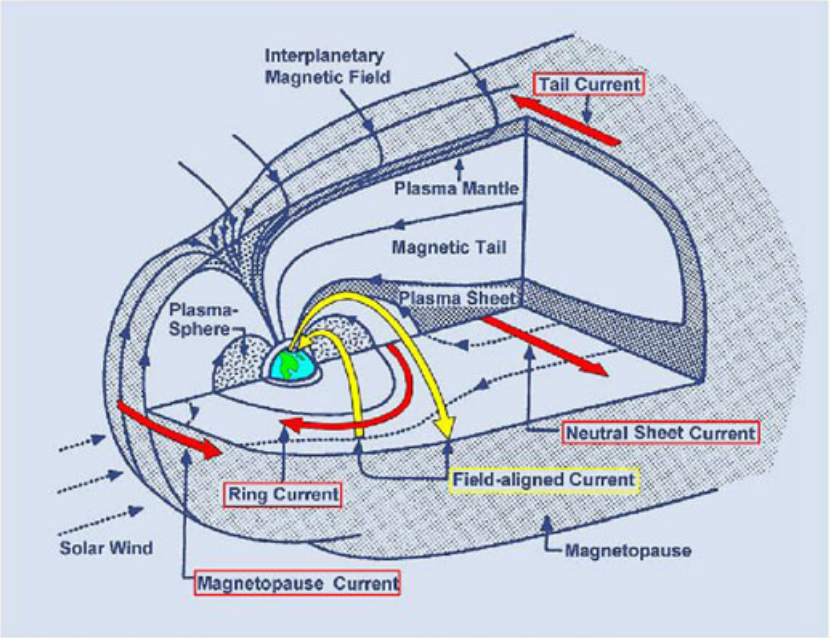

Fig. 5–Magnetospheric currents [21].

periodicity that is related to the 27-day rotation period of the sun. They are strongly influenced by the surface activity of the sun. Maximum activity occurs during the spring and fall when Earth is at the equinoxes. The magnetic field induced by the auroral currents can be much stronger than the other ionospheric current systems. Typical variations are on the order of 1500 nT. This indicates that navigation near Earth's poles may potentially be difficult [19].

Earth's magnetosphere is the area of space surrounding Earth in which charged particles from the sun interact with Earth's magnetic field. The currents of the magnetosphere are driven primarily by the solar wind coming from the sun. The solar wind is a stream of plasma ejected from the sun at high velocities. This stream of particles is composed of electrons and protons. When these charged particles reach Earth they begin to interact with Earth's magnetic field. These interactions can cause currents that create their own magnetic fields. The magnetosphere field is primarily driven by ring currents and the currents of the magnetopause and magnetotail. Figure 5 shows a depiction of the major current systems of the magnetosphere. Ring currents are the most prominent current systems in the inner magnetosphere [20]. Ring currents are caused by currents that flow along the magnetopause. These

currents cancel Earth's field outside the magnetopause boundary and stretch the field outward in the characteristic tail shape [15]. The resulting cavity contains sheet currents that are aligned with the equatorial plane. These currents interact with radiation belts near Earth and create ring currents, which partially circle Earth [15]. The ring currents achieve full loop closure by coupling with the ionosphere. These coupling currents are described shortly. The combined effect of the ring currents and the magnetopause and magnetotail currents is approximately 20–30 nT during quiet times but can be in the hundreds of nT during geomagnetic storms [15].

The previously described magnetosphere currents are roughly solenoidal [15]. This means they tend to flow in closed paths. Because of the variable conductive structure of the near-Earth region, this closure is sometimes achieved through the coupling of the magnetosphere sources and the ionosphere sources [15]. The coupling of sources to close a current loop forms another distinct magnetic source. When this coupling takes place near Earth's poles, it is called a field-aligned current (FAC). This name comes from the fact that Earth magnetic field lines are vertical near its poles so the coupling currents are flowing along the main Earth magnetic field lines. During quiet periods at high latitudes, FACs create magnetic fields on the order of 30–100 nT [15]. There are also coupling currents that flow between the magnetosphere and the Sq currents. These induce a magnetic field with a magnitude of around 10 nT or less. Finally, the equatorial electrojet can also couple with the magnetosphere with currents causing a magnetic field on the order of 15–40 nT [15]. The FAC is another contributing factor to the highly varying fields near Earth's poles and another reason why magnetic navigation near the poles would be difficult.

Proposed Navigation Signal

As previously mentioned, Earth's crustal field shows promise as a navigation signal. Unfortunately, there is no way to directly measure the crustal field. Only total magnetic intensity, which is the superposition of all magnetic sources, can be measured. The proposed navigation signal is instead the magnetic anomaly field. The magnetic anomaly field is defined as the signal obtained by differencing measurements of the total field with a reference field and removing the time-varying external sources. In practice, the reference field is usually the International Geomagnetic Reference field, or IGRF. The IGRF primarily captures Earth's time-varying core field. In an aeromagnetic survey, temporal variations are usually removed by the use of a stationary magnetic base station within the region being mapped (in this research, we propose a real-time way of accomplishing this removal without a base station). Because the crustal field is largely an induced field pointing in the same direction as the IGRF field [17], this scalar subtraction of vector fields is valid, and the result is a map that primarily captures the crustal field. The accuracy of obtaining the crustal field from this scalar subtraction is not actually an issue for the proposed navigation system, because it is the anomaly field itself that will be used for navigation. We only stress the relationship between the crustal and magnetic anomaly fields to emphasize the previously mentioned desirable qualities of the crustal field as a navigation signal – namely, the high spatial-frequency content and the near-static nature of the signal.

Using magnetic anomaly maps to navigate requires measuring the magnetic anomaly in real time. This requires the removal of both the IGRF, as well as the external temporal variations. Removing the IGRF in real time is not difficult. This field is well modeled, with an update every five years, and includes time derivative terms to account for changes over time [14]. This field also has low spatial variability, so any errors in this removal process will appear as a constant bias that is easy to estimate and remove. Estimating and removing the temporal variations is more difficult and addressed in the section 'Removing Temporal Variations.'

Claiming the magnetic anomaly field is static over time requires explanation of a subtlety regarding the crustal field. The crustal field is primarily an induced field. The inducing field (the IGRF) is slowly changing over time, so the crustal field will change slowly as well. The distribution of susceptible magnetic materials in the ground has not changed, however. It is a common practice for geophysicists to perform an operation known as a reduction to the pole [14]. This operation transforms a magnetic anomaly map to what it would look like if the distribution of magnetic materials had been at the magnetic pole. They also perform similar operations to combine magnetic anomaly maps created at different times [14]. Fundamentally, all the information needed to know what the field looks like under various inducing fields is captured in a single map because the magnetic distributions are static. Transforming magnetic anomaly maps to reflect various inducing fields is well understood. To achieve the best accuracies when navigating using magnetic anomaly maps, the maps must be projected forward in time to reflect what they look like under the current IGRF.

Removing Temporal Variations

Any magnetic measurement made in the vicinity of Earth will include the superposition of all of the

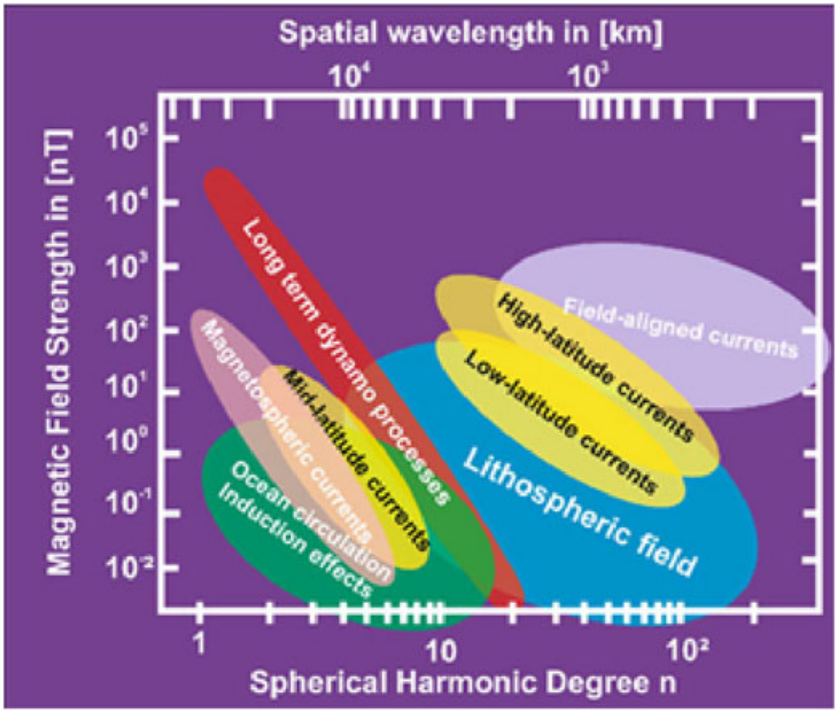

Fig. 6–Frequency content vs. amplitude [17].

discussed magnetic sources. In the context of navigating with Earth's magnetic anomaly field, external time varying-sources corrupt the signal. If the magnetic anomaly field is to be used for navigation at the highest possible accuracy, these time and spatially varying signals need to be removed. Figure 6 shows a summary of spatial wavelength versus amplitude of many of the discussed magnetic field sources at 400 km altitude. Because of the altitude the figure represents, the shortest wavelength of the lithospheric (crustal) field is 200 km. As discussed previously, at aircraft altitudes, these wavelengths would be far shorter (and conversely, frequencies would be higher). Of particularly important note in Figure 6 is the maximum spatial-frequency content of the time-varying magnetic sources. It is clear that at aircraft altitudes, the spatial-frequency information of the crustal field is far higher (shorter wavelength) than any of the other sources. This is helpful for navigation because it means the corrupting signals (anything besides the crustal field) have limited spatial-frequency overlap with the signal use for navigation.

Many of the external magnetic sources also change with time. When flying over a spatial map at a given velocity, the spatial frequencies from the crustal field are manifested as temporal frequencies in the measurements. Observability of the crustal field is hindered if these temporal frequencies overlap with the temporal frequencies of the external magnetic sources. A simple approximation to determine the expected crustal field spatial frequencies is to observe the line spacing requirements for aeromagnetic surveys. Reid [12] showed that the aliased power ($F_{aliased}$) expected from an aeromagnetic survey at height h and line spacing Δx is given by

Table 1 — Height/line spacing ratio vs. aliased power [12]

Height/line spacing	Percent aliased power (%)
0.25	21
0.5	4.3
1	0.19
2	3e-4

$$F_{aliased} = e^{\frac{-2\pi h}{\Delta x}} \tag{1}$$

Table 1 shows the aliased power given by Equation (1) for several ratios of height and sample spacing. As shown in Table 1, when sampling the magnetic field during an aeromagnetic survey, nearly 100 percent of the signal is captured if the sample spacing is one half that of the height. This fact, along with the Nyquist frequency theorem, indicates the shortest expected wavelength at a given height h is itself h. Spatial frequencies then manifest themselves as temporal frequencies according to

$$F_{time(max)} = \frac{1}{h} V_t \tag{2}$$

where h is height and V_t is total velocity. Table 2 shows a general range of expected temporal-frequencies from flying over the crustal field, given by Equation (2). As seen in Table 2, the maximum

Table 2 — Max crustal field temporal frequencies when sampled from an aircraft

	50 m/s (Hz)	100 m/s (Hz)	500 m/s (Hz)
500 m	0.1	0.2	1
1 km	0.05	0.1	0.5
5 km	0.01	0.02	0.1
10 km	0.005	0.01	0.05

frequencies range from 1 Hz when flying low and fast, to 0.005 Hz when flying high and slow. Comparing these temporal frequencies expected when flying over the crustal field to Figure 2 indicates that the temporal frequencies of the external magnetic sources do overlap with the temporal frequencies of the crustal field seen at aircraft altitudes and velocities. It is important to note that we would not expect observability of temporal variations at these frequencies. However, the magnitude of temporal variations at these overlapped frequencies is generally less than the accuracy of the sensor. Although the signal is being corrupted at these frequencies, the absolute accuracy of the measurements is relatively unchanged. This analysis of spatial and temporal frequencies of the crustal field compared to other magnetic sources indicates that separating these sources while flying at aircraft velocities and speeds should be possible to some extent. This lends further evidence to the crustal field being a viable navigation signal.

NAVIGATION FILTER FRAMEWORK

The overall structure of the proposed navigation filter is that of a particle filter. The particle filter lends itself well to map-based navigation. Many alternative methods exist for contour matching-type algorithms. Terrain-following systems such as SITAN, which use terrain maps and radar/laser altimeters, are likely the most well-known implementation of these types of algorithms [10]. They all share the common idea of matching a sequence of measurements to an area of a map where there exist similar expected measurements. Because the actual magnetic field is always changing with time, a particle filter is a useful alternative to these batch-type estimators because it allows simultaneous estimation of the temporal variations. Magnetic anomaly navigation also lends itself to a particle filter approach because the magnetic map can be interpolated to a continuous map. Individual measurements can be used to update the filter, unlike batch approaches. Another possible method is a Kalman Filter approach. Kalman Filter frameworks require a mathematical model to relate the measurements to the filter states. Aeromagnetic surveys exist as gridded maps of data points. While spherical harmonic models of Earth's magnetic field exist for the low-frequency components of the magnetic field, no such models, which include the needed high frequency components, are readily available for a multitude of regions (although this would be an interesting approach to study). Particle filters can work in real time, easily handle the matching of measurements to a gridded map, and can also simultaneously estimate the time varying components of the external magnetic field.

A five-state particle filter was designed for magnetic anomaly field navigation. The first four states are error states of an inertial navigation system. These include latitude and longitude error, as well as north and east velocity error. The final state can either be the estimated temporal variation, or the residual of the temporal variations after removing a model's estimated value. The temporal variation (T_V) state is treated as a first order Gauss–Markov (FOGM) process. Barometric aiding to bound altitude error occurs inside the INS mechanization equations, not in the filter. Each particle in the particle filter is represented by these five states. The states are

$$\widehat{\boldsymbol{x}} = \begin{bmatrix} \delta_{lat} \\ \delta_{lon} \\ \delta_{vn} \\ \delta_{ve} \\ T_V \end{bmatrix} \tag{3}$$

The dynamics model for the states is a standard INS error model (Pinson Error Model, see [22]) truncated to include only the latitude, longitude, and north and east velocity terms. Also included is a FOGM state for the temporal variations, described later. The dynamics model is given by

$$\mathbf{F} = \begin{bmatrix} 0 & 0 & \frac{1}{r_{earth}} & 0 & 0 \\ \frac{v_e tan(L)}{r_{earth} cos(L)} & 0 & 0 & \frac{1}{r_{earth} cos(L)} & 0 \\ \mathbf{A} & 0 & \frac{v_d}{r_{earth}} & \mathbf{B} & 0 \\ \mathbf{C} & 0 & \mathbf{D} & \frac{v_e tan(L)+v_d}{r_{earth}} & 0 \\ 0 & 0 & 0 & 0 & \frac{-1}{\tau} \end{bmatrix} \tag{4}$$

where:

$$\mathbf{A} = -v_e \left(2\Omega cos(L) + \frac{v_e}{r_{earth} cos^2(L)} \right) \tag{5}$$

$$\mathbf{B} = -2 \left(\Omega sin(L) + \frac{v_e tan(L)}{r_{earth}} \right) \tag{6}$$

$$\mathbf{C} = 2\Omega (v_n cos(L) - v_d sin(L)) + \frac{v_n v_e}{r_{earth} cos^2(L)} \tag{7}$$

$$\mathbf{D} = 2\Omega sin(L) + \frac{v_e tan(L)}{r_{earth}} \tag{8}$$

and:

R_{earth} = Radius of Earth
Ω = Rotation Rate of Earth
L = Latitude
v_n, v_e, v_d = North, East, and Down velocities

The particle filter framework consists of an initialization step followed by a loop of three main tasks: propagation of the dynamics model, weighting of the particles using a magnetic field measurement, and stochastic resampling. These will be discussed in the sections that follow.

Initialization

The particle filter is initialized by generating N particles based on previously known statistics regarding the state variables. The value of N can vary widely – in this research, we used $N = 1,000$ particles. In our simulation, described shortly, the statistics are assumed to be from a Global Positioning System (GPS)/INS hybrid system that has recently lost GPS lock. In this case, an INS system's solution begins to accumulate errors, but maintains statistical estimates of the position, velocity, and attitude errors. These statistics could be used to initialize the filter states assuming a Gaussian model. In this way, there are N hypotheses of various INS error state combinations, some of which are likely to be correct. The temporal variation state can be initialized by known statistics as well – this topic has a dedicated section later in the paper. Note that the filter could use a map-wide initialization in which the aircraft could be anywhere over a large region of the map. In this case, the initial solution would be multimodal for a short period of time before converging to a uni-modal solution.

Particle Propagation

At a chosen interval the filter will propagate the particles forward in time. In a particle filter, this includes adding driving noise to certain states to cause the particles to drift. With only four INS error states, the noise is added to the velocity states. In this way, it acts as a velocity random walk (VRW) term, which is large enough to capture the drift of all INS error sources. The temporal variation state also has a driving noise added, but again this is discussed in detail later. Propagation of each of the N particles takes the form

$$\widehat{\mathbf{x}}_{p_{t+1}} = \boldsymbol{\phi}\widehat{\mathbf{x}}_{p_t} + \mathbf{Q_d} \tag{9}$$

where:

$\boldsymbol{\phi}$ is the discretized dynamics matrix, $\mathbf{F}$;
$\mathbf{Q_d}$ is the discretized noise vector, $\mathbf{Q}$; and
$\mathbf{x_p}$ is the particle state.

The $\mathbf{Q}$ matrix is given by:

$$\mathbf{Q} = \begin{bmatrix} 0 \\ 0 \\ VRW_n \\ VRW_e \\ \frac{2\sigma^2}{\tau} \end{bmatrix} \tag{10}$$

where:

VRW_n and VRW_e are the north and east VRW terms;
σ is the temporal variation FOGM strength; and
τ is the temporal variation FOGM time constant.

The VRW terms are best derived empirically for a given INS.

Particle Weighting

When a measurement comes into the filter, each particle is weighted using the new measurement. This weighting process assumes a Gaussian distribution of measurement errors and is given by

$$P_W = \frac{1}{\sqrt{2\pi R}} exp\left(-\frac{(Z(t) - (M(x_{ins}) + O_B(t) + P_M))^2}{2R}\right) \tag{11}$$

where:

P_w is the particle's weight;
R is the measurement noise of the OPC magnetometer;
$Z(t)$ is the measurement of the OPC magnetometer;
$M(x_{ins})$ is a reference field model such as the IGRF (function of ins position estimate);
P_m is the expected magnetic intensity based upon the particle's state; and
$O_B(t)$ is the pre-computed 24-h temporal variation baseline (used to improve the assumption that temporal variations can be modeled as a FOGM process).

Existing magnetic anomaly maps usually have the main/core field removed using a reference model. Recall that the main field accounts for about 95 percent of the measured field, has low-frequency variations, and drifts over time. Therefore, to match the magnetic map, the measurements also must have this field removed. Alternatively, the reference field may be added back to the magnetic anomaly map. In either case, it is important to use the same reference model which was used in creating the magnetic anomaly map, and ensure the model accounts for secular variations in the main field (includes time derivative terms). The $O_B(t)$ term is the average diurnal cycle mentioned previously – a pre-computed 24-h curve, which enables the temporal variations to be more accurately modeled as

a FOGM process. Subtracting the diurnal average causes the temporal variations to be better approximated as a zero-mean process. The value for P_m is derived from the particle's state and includes a magnetic intensity based on hypothesized location and the hypothesized temporal variation. In practice, there needs to be a quick way to associate a latitude and longitude with an expected magnetic intensity. We used a bivariate spline approximation over a rectangular mesh from Python's SciPy library to interpolate a magnetic field value for any given latitude and longitude [23]. Any robust interpolation method would suffice. P_m is then

$$P_m = I_{map} + I_{temporal} \tag{12}$$

where:

P_m is the expected magnetic intensity measurement for an individual particle; I_{map} is the interpolated value from the gridded magnetic field map based on the particle's latitude and longitude; and

$I_{temporal}$ is the particles hypothesized temporal variation.

After the particles are weighted, they are normalized to all sum to one. This allows a simple weighted sum of the particles to obtain a single estimate of the aircraft's position and velocity, as well as the current temporal variation value. The standard deviation of the particles is used to determine an uncertainty bound.

Stochastic Resampling

A well-known characteristic of particle filters is the risk of particle starvation. This occurs when only a few particles begin to have any significant weight, as all of the other particles diverge. There are many methods of stochastic resampling and any robust method would suffice. We used the sequential importance resampling approach [24] and found resampling after each measurement produced the best results.

ESTIMATION OF TEMPORAL VARIATIONS

Perhaps the most significant hurdle in achieving high accuracy in magnetic anomaly navigation is the estimation of temporal variations. As the name suggests, these variations occur in the magnetic field temporally, but it is important to note they corrupt the navigation signal spatially as well. This challenge is unique to magnetic field navigation. In terrain and gravity systems, the signal being used for navigation is not generally corrupted with another signal varying with time and location. Figure 7 shows a magnetic anomaly map over the American Midwest. Between the lightest and darkest areas of the map, the magnetic field changes by about 700 nT. Even on a magnetically quiet day, the magnetic field can change by 50 nT in the span of a few hours. During a magnetic storm, the field can change by hundreds of nT. Even in a magnetic storm, a properly tuned filter should not diverge. Rather, the high temporal variations degrade filter accuracy and increase the uncertainty of the estimated solution. The first step in modeling the temporal variations is understanding the major variables that effect these variations. The presented variables are far from an exhaustive list, but allow for an adequate filter model. In the sections that follow, local time, latitude, and magnetic storm indices are analyzed. A full model might also include longitude, season or time of year, F10.7 ionospheric index, sunspot number, and mantle conductivity, but these are not covered in this paper.

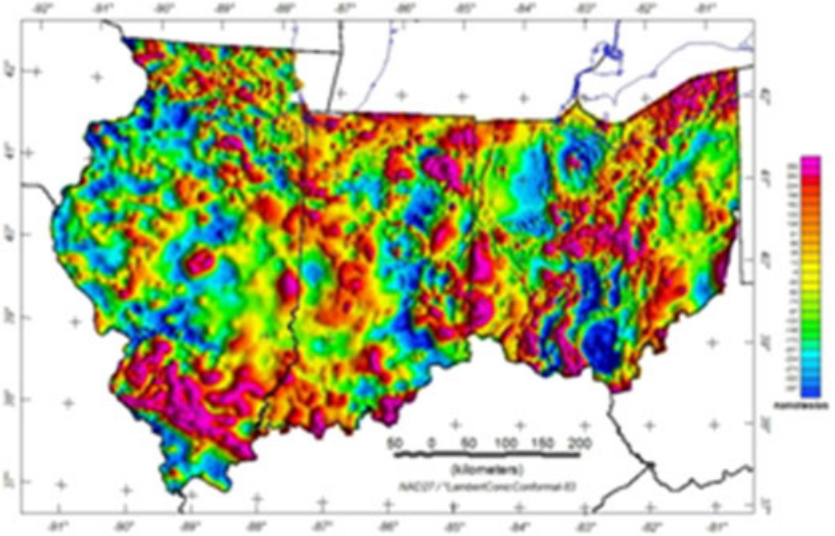

Fig. 7–Midwest magnetic anomaly field [25].

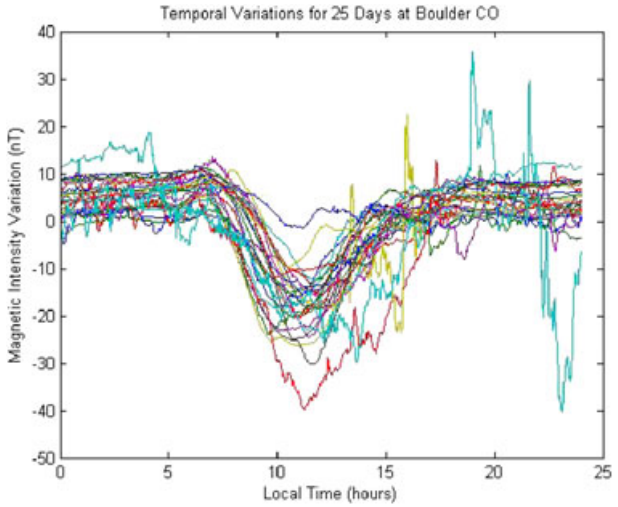

Fig. 8–25 Days of temporal variations at Boulder CO Observatory (October, 2013).

Time Dependence of Temporal Variations

Under quiet conditions, the greatest predictor of the temporal variation's value is local time. During an aircraft flight, this variable changes not just from the passage of time, but also from traversing the globe longitudinally. As described previously, these changes in the temporal variations are driven by Earth rotating with respect to a stationary ionospheric current system. Recorded temporal variation data was obtained from the United States Geological Survey [25]. Figure 8 shows the temporal variations for 25 consecutive days at a magnetic observatory in Boulder, CO. At this particular observatory, it can be seen that during the daytime the magnetic field dips down, with the minimum value reached around 11 am. This periodic behavior of the temporal variations is seen all over the world, but less so at the poles. In equatorial regions, the midday value is a maximum instead of a minimum. One possible insight from the time dependence of the temporal variations is that nighttime navigation using the magnetic anomaly field may be more accurate than daytime navigation. It is important to note that this is not because of the max/min that occurs at mid day, but rather because the temporal variations tend to have lower frequency information at nighttime.

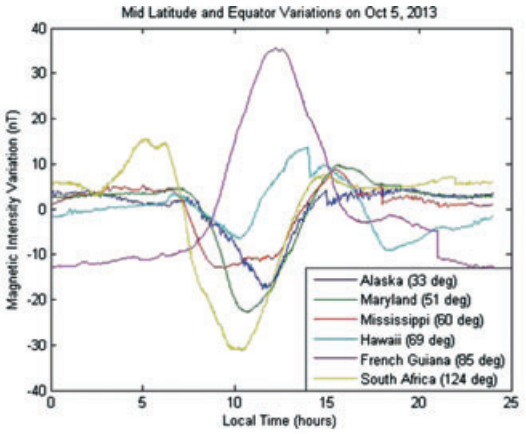

(a) Equatorial and Mid latitude Variations on Oct 5, 2013

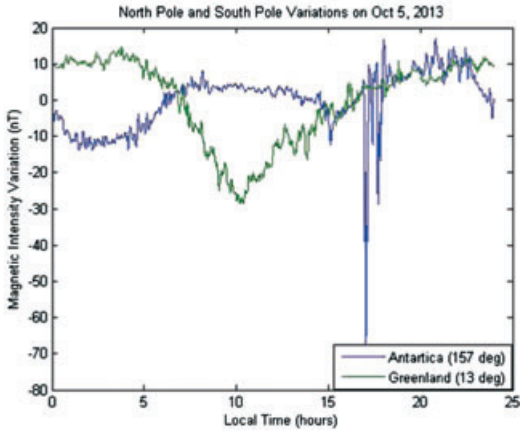

(b) North and South Pole Variations on Oct 5, 2013

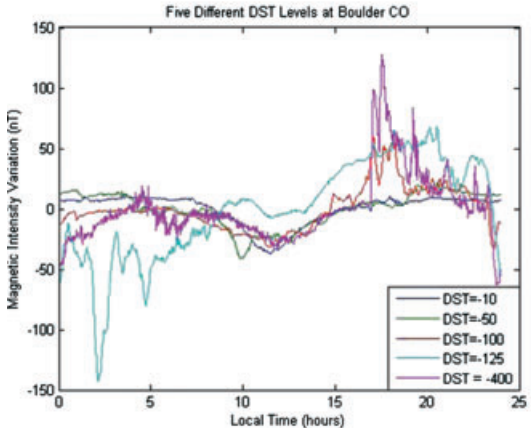

(c) Five Different DST Levels at Boulder CO (various days)

Fig. 9–Observatory data.

Latitude Dependence of Temporal Variations

The temporal variations also change based on latitude. The mid-latitudes generally have the quietest magnetic conditions, and when adjusted for local time, these variations are similar at varying locations. The equatorial regions have stronger variations, which can be opposite in sign because of the equatorial electrojet (Figure 4). The poles have much greater variations. Figure 9a shows the temporal variations at five different magnetic observatories on the same day and with the same local time. Four of the observatories are from mid-latitude regions and the fifth is from an equatorial region. Notice the opposite sign on the French Guiana data, which is near the equator, and the

slight rise in Hawaii, which is much closer to the equator than the other observatories. (Latitudes are given as co-latitudes where 0 deg is the North Pole and 180 deg is the South Pole.) Much greater variations are possible near Earth's poles. As described previously, this is caused by a wide variety of effects such as the presence of field-aligned currents [19].

Figure 9b shows the recorded temporal variations for the same day as the previous figures in Antarctica and Greenland. Notice the sharp pulsation that occurs around 1600 h in Antarctica. It is clear from the previous two figures that the variations at the poles are much less smooth than the variations at the equator and mid-latitude regions. This indicates that magnetic navigation near the poles may be less accurate than at mid-latitudes and equatorial regions.

Magnetic Storm Conditions

The final variable, which will be observed, is magnetic storm conditions. Magnetic storm conditions are characterized with the Disturbance Storm Time, or DST index. The DST index is a single number that applies globally to Earth's magnetic field and gives a measurement of the strength of the magnetosphere ring current [26]. It is helpful in indicating when magnetic storms are likely. There is a very clear divide between magnetically quiet days and stormy days. The temporal variations during the quietest days of a month can be remarkably consistent. When a magnetic storm hits, however, the variations can be drastically different. This makes DST index a useful variable to test against in developing a navigation filter. The filter should be able to operate on days with varying magnetic storm conditions, and we will show later that our proposed solution does. Figure 9c shows five different days with increasing DST indices at the magnetic observatory in Boulder, Co.

Temporal Variation Parameterization

We suggest a straightforward approach for the modeling of temporal variations. This approach would likely be limited to non-polar regions. We wish to model the temporal variations as an FOGM process. As shown in Figure 8, the large noon-time swings are not representative of a FOGM process, so, they must be removed. Most magnetic observatories record monthly baseline averages for solar quiet days. These averages are normally obtained by selecting the five 'quietest' days of a month. Figure 10a shows five quiet days from the Boulder observatory in October 2010, as well as their mean. This mean is a time-dependent function that estimates the baseline temporal variations for a given month in a given region. The region for which this baseline would be accurate would be fairly large, and the current distribution of magnetic observatories around the world suggests this approach is feasible. An aircraft in flight could have these monthly

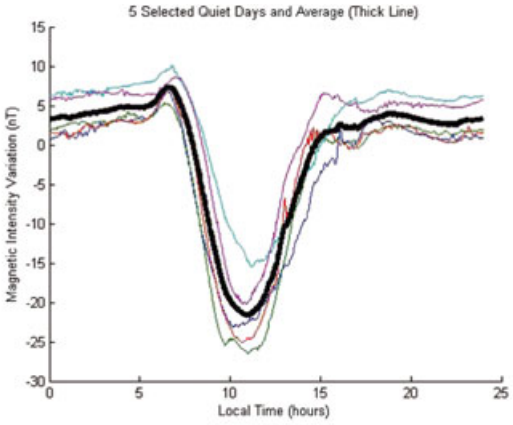

(a) Selected Quiet Days and Average from Oct. 2013 at Boulder, CO

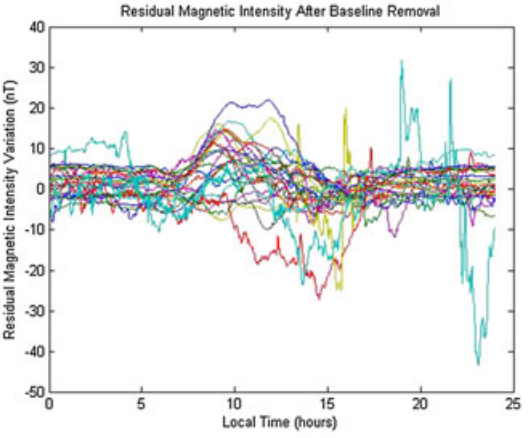

(b) Residual Magnetic Intensity from 25 days at Boulder, CO Observatory

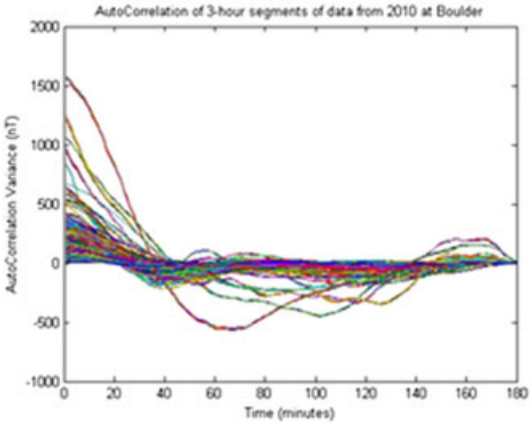

(c) Auto-Correlations of Temporal Variation Residuals (Monthly Means Removed)

Fig. 10–First-order Gauss–Markov (FOGM) analysis.

averages stored in a database and use them to remove a baseline estimate of the temporal variations. The navigation filter may have to access several of these stored baselines within a single flight if flying long distances. These baselines would be a function of local time. The residual temporal variations that remain after subtracting the baselines are more representative of an FOGM process, as shown in Figure 10b.

The last step in modeling the temporal variations is to estimate the statistics of the FOGM process. This was accomplished by looking at a large data set and computing autocorrelations. We took an entire year's worth of data from the observatory at Boulder, CO, and broke it into 3-h segments with the baseline estimate removed. We then performed an autocorrelation on each of these 2920 3-h segments, shown in Figure 10c. Because these curves can be roughly modeled as a decaying exponential, we can fit an FOGM process to them. As shown in Figure 10c, the vast majority of the 3-h segments have a σ less than 25 nT – approximately 98 percent of the segments. The most useful predictor variable of the σ and τ values was the σ and τ values from the previous 3-h time segment. For short duration flights using the last known value is effective, but for longer duration flights it may be better to use an average value. We considered the DST index for predicting the FOGM σ and τ values but found very little correlation.

Simulation

We implemented the previously described filter framework in a navigation simulation. For the magnetic map, we used a high-resolution aerial survey over the state of Ohio, obtained from the United States Geological Survey [25]. For our inertial navigation data and GPS truth data, we used real data from a previous flight test over the mapped area. It is important to note the flight trajectory traverses a relatively benign part of the magnetic anomaly map and improved performance would be expected over areas of higher magnetic gradients. The only artificial data in the simulation was the OPC magnetometer measurements. These were synthesized from two sources – the true magnetic map values for the given location corrupted with an instrument error model as well as a 3-h segment of recorded temporal variations from the Boulder CO observatory in October 2010. The instrument error model contained a heading dependent scale factor term, a moving bias term, and a sensitivity (white noise) term. These are the dominant errors of an OPC magnetometer. These errors contribute to the overall absolute accuracy of the instrument, which is better than 1 nT [6]. The measurements were corrupted with both stormy and quiet condition temporal variations. Figure 11 shows the flight path of the aircraft over the high-resolution magnetic map. A circle drawn to approximate scale is drawn around the major city of Columbus, Ohio, suggesting the crustal field, not man-made noise, dominates the signals.

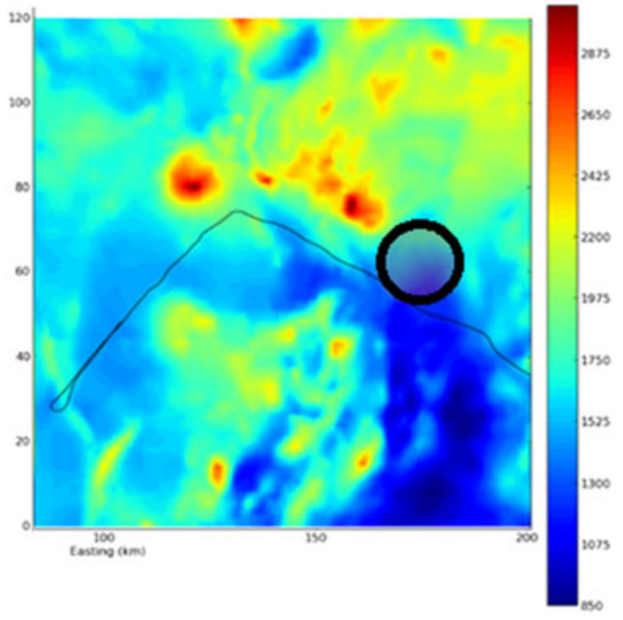

Fig. 11–High resolution magnetic anomaly map over Ohio and flight path.

Results

The nominal test case involved flying at the mapped altitude (500 m) under quiet conditions using a navigation-grade INS. Figure 12a shows the horizontal RMS errors as a function of time. The total RMS error of this flight was 20 m. Figure 12b shows the filter has observability of the temporal variations. Figure 12c shows the filter has observability of the velocity errors as well.

Filter accuracy is clearly dependent on altitude, as increasing altitude essentially acts as a low pass filter on the spatial map. We computed an upward continuation of the mapped data from the altitude of 500 m. See Blakely [11] for details on how to perform an upward continuation of magnetic map data, including a sample code snippet. Figure 13 shows the mapped region at three progressively higher altitudes. It is clear that the well-defined features at low altitudes begin to blur together. We ran the filter simulation at five different altitudes under magnetically quiet conditions. Table 3 shows the results of this trade-space analysis. As expected, filter accuracy begins to degrade as altitude is increased. Even at 30,000 ft, however, the filter has still not diverged and has accurate covariance bounds on its position estimate. It is important to note

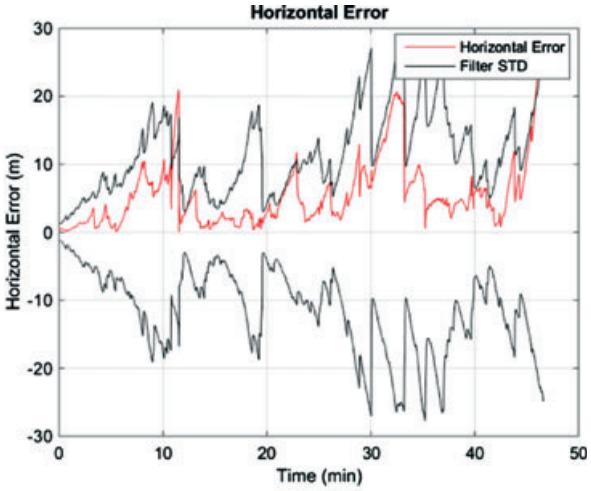

(a) Horizontal Filter Error for Nominal Case

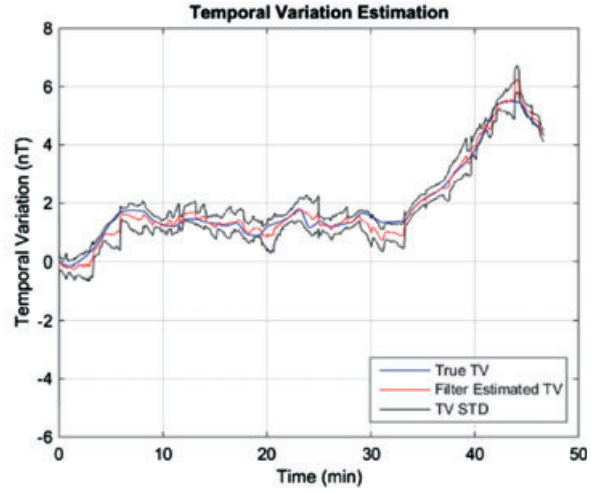

(b) Filter Tracking of Temporal Variations

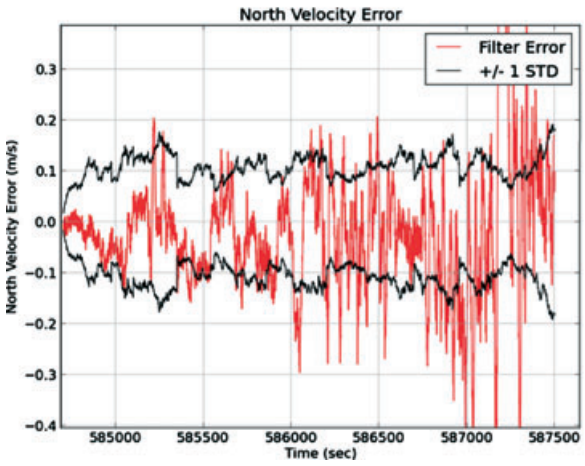

(c) North Velocity Error for Nominal Case

Fig. 12–Simulation results.

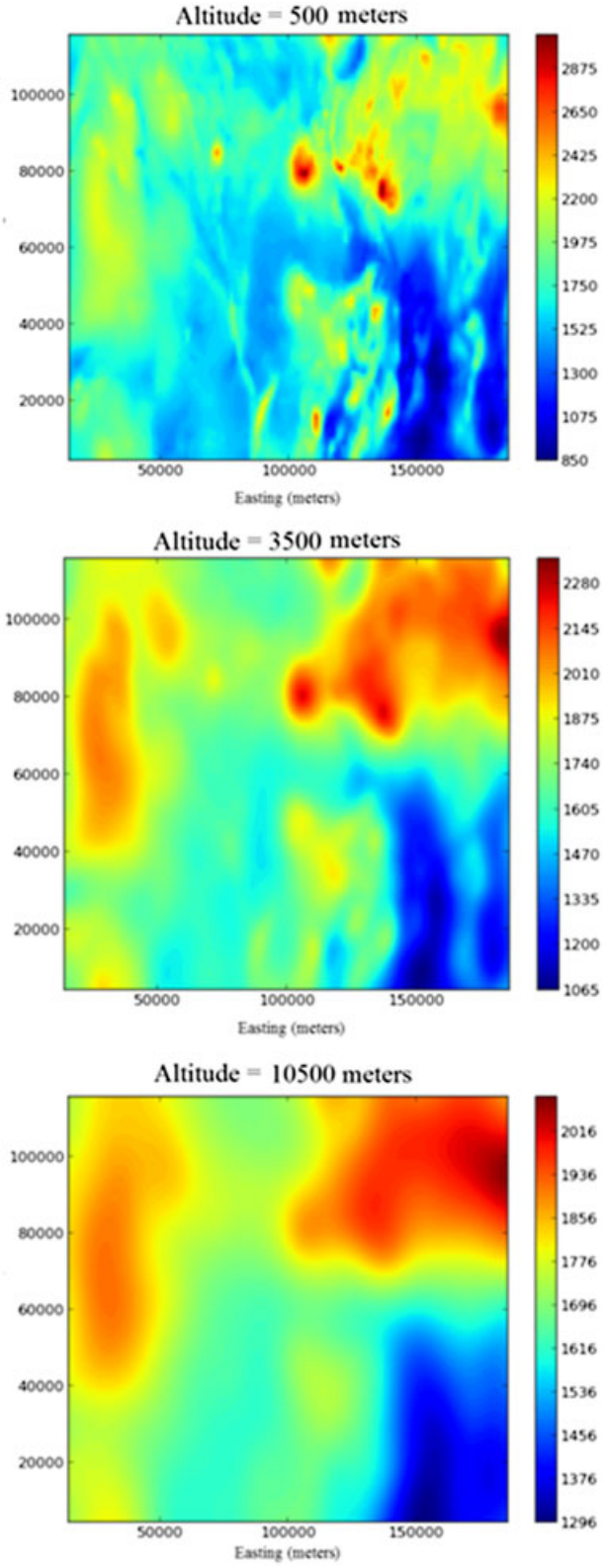

Fig. 13–Upward continuation of mapped data.

that the altitude variable is altitude above terrain, so ocean depth would contribute to total altitude when flying over oceans.

Next, a trade-space analysis was performed on magnetic storm conditions. The simulation was run at an altitude of 500 m with a navigation-grade INS. We ran the filter against all 2920 3-h segments of

Table 3 — Altitude tradespace on filter accuracy

Altitude	Horizontal root mean square error (meters)
500 m	20
1 km	45
3.5 km	139
5 km	156
10 km	171

Table 4 — Comparison of filter accuracy under quiet and stormy conditions

Quiet horizontal error	Stormy horizontal error
21.51 m	30.66 m

data from Boulder, CO to capture the effects of various magnetic storm conditions. For these tests, we tried using both the previous values of σ and τ as well as the average values for the FOGM parameters. We determined that there was only a small improvement using the last known σ and τ values over using the average values. We also determined that under magnetic storm conditions the filter RMS error increases. We defined magnetic storm conditions as having a Kp index of 3 or higher. The Kp index is similar to the DST index but is a simpler metric that ranges from 0–9, where 9 is the strongest magnetic storm conditions. We broke the 2920 3-h segments into 'quiet' and 'stormy' conditions based on the Kp index metric, and took the average horizontal RMS error over all the runs in each category. The stormy days made up 13 percent of the runs and the quiet days made up the other 87 percent of the runs. Magnetic storm conditions decreased filter performance, as shown in Table 4. This decrease in accuracy was small compared to changes in altitude and would not likely be the dominant source of error in a flight. Finally, we would like to emphasize that although the filter does not depend much on magnetic storm conditions or the method of estimating the FOGM parameters, the estimation of the temporal variations is still vital. Navigation accuracy decreases by an order of magnitude when the temporal variations are not estimated and removed.

CONCLUSIONS

This paper presented a method for implementing an alternative navigation system using measurements from an OPC magnetometer and a high-resolution magnetic anomaly map. We presented a background on the components of a magnetic measurement in the vicinity of Earth. We motivate the fact that the magnetic anomaly field is a useful signal for navigation and can be observed even in the presence of the main Earth field and temporal variations. We propose methods to remove the corrupting temporal variations to improve accuracy. A global (non-polar) filter framework is proposed using a particle filter. We show 20 m absolute accuracies at low altitudes under quiet conditions and a few hundred meter accuracy at high altitudes. We address the concerns of magnetic storms by showing the filter functioning throughout an entire year's worth of magnetic storm conditions. Navigation with the magnetic anomaly field shows promise to be a robust worldwide source of absolute positioning information.

DISCLAMER

The views expressed in this paper are those of the authors and do not reflect the official policy or position of the United States Air Force, Department of Defense, or U.S. Government.

REFERENCES

1. Storms, W., and Shockley, J., "Magnetic Field Navigation in an Indoor Environment," *Ubiquitous Positioning Indoor Navigation and Location Based Service (UPINLBS)*, IEEE, 2010, pp. 1–10.
2. Haverinen, J., et al., "A Global Self-Localization Technique Utilyzing Local Anmolies of the Ambient Magnetic Field," *Proceedings of IEEE International Conference on Robotics and Automation*, Kobe International Conference Center, Kobe, Japan, 2009.
3. Schockley, J., *Ground Vehicle Navigation using Magnetic Field Variation,* Dissertation, Air Force Institute of Technology, 2012.
4. Psiaki, F. S., et al., "Ground Tests of Magnetometer-based Autonomous Navigation (magnav) for Low-Earth-Orbiting Spacecraft," *Journal Of Guidance, Control, and Dynamics*, Vol. 16, No. 1, 1993, pp. 206–14.
5. Wilson, J. M., and Kline-Schoder, R., "Passive Navigation using Local Magnetic Field Variations," *Proceedings of the 2006 National Technical Meeting of The Institute of Navigation*, Monterey, CA, January 2006, pp. 770–779.
6. Hood, P., "History of Aeromagnetic Surveying in Canada," *The Leading Edge*, Vol. 26, No. 11, 2007, pp. 1384–1392.
7. Yi, L. Y., et al., "A New Correlation Matching Algorithm based on Differential Evolution of Geomagnetic Aid Navigation," *Applied Mechanics and Materials*, Vol. 2032, No. 038, 2011, pp. 94–96.
8. Li, M., et al., "Novel Algorithm for Geomagnetic Navigation," *Journal of Central South University of Technology*, Vol. 18, 2011, pp. 791–799.
9. Caifa, G., and Anlian, L., "Algorithm for Geomagnetic Navigation and its Validity Evaluation, College of Aerospace and Materials Engineering," National University of Defence Technology.
10. Hostetler, L., and Andreas, R., "Nonlinear Kalman Filtering Techniques for Terrain-aided Navigation," *IEEE Transactions on Automated Control*, Vol. 28, No. 3, 1983, pp. 315–323.

11. Blakely, R. J., *Potential Theory in Gravity and Magnetic Applications,* Cambridge, 1996.
12. Reid, A. B., "Aeromagnetic Survey Design," *Geophysics*, Vol. 45, No. 5, 1980, pp. 937–976.
13. DeGregoria, A., *Gravity Gradiometry and Map Matching: An Aid to Aircraft Inertial Navigation Systems,* Thesis, Air Force Insitute of Technology, March 2010.
14. Hinze, W. J., and Von Frese, R., *Gravity and Magnetic Exploration: Principles, Practices, and Applications,* Cambridge, 2013.
15. Sabaka, O. N., et al., "A Comprehensive Model of the Quiet-Time, Near-Earth Magnetic Field: Phase 3," *Geophysical Journal International*, Vol. 151, No. 1, 2002, pp. 32–68.
16. Hulot, G., "Terrestrial Magnetism," *Space Science Series of ISSI,* Springer, 2011.
17. Cain, J., and Blakely, R., "The Magnetic Field of the Earth's Lithosphere: The Satellite Perspective," *EOS, Transactions American Geophysical Union*, Vol. 80.14, No. 156, 1999.
18. Marshall, R., "Geomagnetic Pulsations in Aeromagnetic Surveys," *Proceedings of NAECON, Magnetic Anomaly Maps and Data for North America*, November 2014.
19. Beck, A. J., "Magnetic Fields - Earth and Extraterrestrial," NASA Space Vehicle Design Criteria [Environment], 1969.
20. Maus, S., and C. Roth, C., "Third Generation of the Potsdam Magnetic Model of the Earth (pomme)," *Geochemistry Journal International*, Vol. 16, No. 1, 2005, pp. 206–214.
21. Kivelson, M., and Russell, C., *A Brief History of Solar Terrestrial Physics*, Cambridge: Cambridge UP, 1995. Ch. Introduction to Space Physics.
22. Titterton, D., and Weston, J. L., *Strapdown Inertial Navigation Technology,* London, UK, 1997.
23. "Scipy Python Library," http://www.scipy.org/, 2014. [Online; accessed 1-Nov-2014].
24. Liu, J. S., and Chen, R., "A Theoretical Framework for Sequential Importance Sampling with Resampling," *Sequential Monte Carlo Methods in Practice*, Springer, 2001, pp. 225–246.
25. USGS, "Magnetic Anomaly Maps and Data for North America", http://mrdata.usgs.gov/magnetic, November 2014.
26. Gonzalez, W. D., "A Study on the Peak DST and Peak Negative BZ Relationship During Intense Geomagnetic Storms," *Geophysical Research Letters*, Vol. 32, No. 18, 2005.